

# Cationic State Distribution over the P700 Chlorophyll Pair in Photosystem I

Keisuke Saito<sup>†</sup> and Hiroshi Ishikita<sup>†‡\*</sup>

<sup>†</sup>Career-Path Promotion Unit for Young Life Scientists, Graduate School of Medicine, Kyoto University, Kyoto, Japan; and <sup>‡</sup>Japan Science and Technology Agency, PRESTO, Saitama, Japan

**ABSTRACT** The primary electron donor P700 in photosystem I is composed of two chlorophylls, P<sub>A</sub> and P<sub>B</sub>. P700 forms the cationic [P<sub>A</sub>/P<sub>B</sub>]<sup>•+</sup> state as a result of light-induced electron transfer. We obtained a P<sub>A</sub><sup>•+</sup>/P<sub>B</sub><sup>•+</sup> ratio of 28:72 and a spin distribution of 22:78 for the entire PSI protein-pigment complex. By considering the influence of the protein components on the redox potential for one-electron oxidation of P<sub>A</sub>/P<sub>B</sub> monomers, we found that the following three factors significantly contributed to a large P<sub>B</sub><sup>•+</sup> population relative to P<sub>A</sub><sup>•+</sup>: 1), Thr-A743 forming a H-bond with P<sub>A</sub>; 2), P<sub>A</sub> as a chlorophyll *a* epimer; and 3), a conserved PsaA/PsaB pair, the Arg-A750/Ser-B734 residue. In addition, 4), the methyl-ester groups of the accessory chlorophylls A<sub>-1A</sub>/A<sub>-1B</sub> significantly stabilized the cationic [P<sub>A</sub>/P<sub>B</sub>]<sup>•+</sup> state and 5), the methyl-ester group orientations were completely different in A<sub>-1A</sub> and A<sub>-1B</sub> as seen in the crystal structure. When the methyl-ester group was rotated, the spin-density distribution over P<sub>A</sub>/P<sub>B</sub> ranged from 22:78 to 15:85.

## INTRODUCTION

In oxygenic photosynthesis, photosystem I (PSI) participates in the conversion of light to chemical energy with photosystem II (PSII). Light-induced electron transfer occurs along a series of cofactors bound to the PsaA and PsaB subunits of PSI. On the lumen side, there exists a chlorophyll dimer P700 composed of two chlorophylls P<sub>A</sub> and P<sub>B</sub>. P<sub>B</sub> is chlorophyll *a* (Chl<sub>a</sub>) and P<sub>A</sub> is Chl<sub>a</sub>′, the C13<sup>2</sup> epimer of Chl<sub>a</sub> (Fig. 1 *a*) (1,2). A second Chl<sub>a</sub> pair next to P<sub>A</sub>/P<sub>B</sub> is the accessory Chl<sub>a</sub> A<sub>-1A</sub>/A<sub>-1B</sub>. In addition, there are two additional distant Chl<sub>a</sub> (A<sub>0</sub>), two phylloquinones (A<sub>1</sub>), and one iron-sulfur cluster (F<sub>X</sub>) in the PsaA/PsaB subunits. Similar to PSII, these six Chl<sub>a</sub> and two phylloquinones are arranged in two electron-transfer branches (A and B), which adopt a pseudo-C<sub>2</sub> symmetry with the rotation axis passing through P<sub>A</sub>/P<sub>B</sub> and F<sub>X</sub>. In PSII, only one of the two branches serves as an electron-transfer active branch; this is in contrast to PSI, in which two branches are electron-transfer active (3), as shown by the biphasic forward electron transfers from P700 to A<sub>1</sub> or from A<sub>1</sub> to F<sub>X</sub> observed in kinetic studies.

The primary process of charge separation culminates with a hole on the P<sub>A</sub>/P<sub>B</sub> pair in PSI or on the P<sub>D1</sub>/P<sub>D2</sub> pair in PSII. In PSII, the cationic state over P<sub>D1</sub>/P<sub>D2</sub> is predominantly observed in the Chl<sub>a</sub> of the electron active branch P<sub>D1</sub>, with a P<sub>D1</sub><sup>•+</sup>/P<sub>D2</sub><sup>•+</sup> ratio of ~80:20 (4,5). For PSI, the P<sub>A</sub><sup>•+</sup>/P<sub>B</sub><sup>•+</sup> ratios or the corresponding spin-density distributions were obtained experimentally by Fourier transform infrared (FTIR) spectroscopy (6) or electron paramagnetic resonance (EPR) (4,7,8) studies, respectively. FTIR studies

indicated that the P<sub>A</sub><sup>•+</sup>/P<sub>B</sub><sup>•+</sup> ratios were in the range of 50:50–33:67 (6). On the other hand, the spin-density distribution over P<sub>A</sub>/P<sub>B</sub> is 25:75 (4) and 25:75–20:80 in PSI from spinach (7) and 15:85 in PSI from *Thermosynechococcus elongatus* (8) (reviewed in Webber and Lubitz (9)).

To understand the role of the amino-acid residues or cofactors of PSI in the energetics of P700, influences of all amino-acid residues and redox-active cofactors on the energetics of P<sub>A</sub>/P<sub>B</sub> Chl<sub>a</sub> monomers as well as the P700 Chl<sub>a</sub> dimer are, for the first time to our knowledge, here elucidated. We present the following: 1), The computational results of the influence of the PSI protein environment on the redox potentials,  $E_m(P_A)$  and  $E_m(P_B)$ , are presented on the basis of the PSI crystal structure (2) in the presence of all protein subunits and cofactors. The linear Poisson-Boltzmann equation is solved by considering the protonation states of all titratable sites in PSI. 2), The P<sub>A</sub><sup>•+</sup>/P<sub>B</sub><sup>•+</sup> ratio for the P<sub>A</sub>/P<sub>B</sub> pair is calculated using a large-scale quantum chemical/molecular mechanical (QM/MM) approach with explicit treatment of the complete PSI atomic coordinates divided into two subsystems; the QM region contains the P<sub>A</sub>/P<sub>B</sub> dimer and is treated by quantum mechanics (unrestricted DFT/B3LYP and LACVP\* level) and the remaining protein subunits and cofactors are treated with the MM force field. The computational conditions and procedures used in studies on the *Thermosynechococcus vulcanus* PSII (10) (using the 1.9 Å structure (11)) were consistently used in our study. This can facilitate the direct analysis and comparison of the influences of protein environments on Chl<sub>a</sub> in both PSI and PSII.

Submitted June 28, 2011, and accepted for publication September 8, 2011.

\*Correspondence: hiro@cp.kyoto-u.ac.jp

This is an Open Access article distributed under the terms of the Creative Commons-Attribution Noncommercial License (<http://creativecommons.org/licenses/by-nc/2.0/>), which permits unrestricted noncommercial use, distribution, and reproduction in any medium, provided the original work is properly cited.

Editor: Leonid S. Brown.

© 2011 by the Biophysical Society  
0006-3495/11/10/2018/8 \$2.00

## EXPERIMENTAL PROCEDURES

In this article, we employed the following systematic modeling procedure:

First, we constructed a realistic molecular model of the whole PSI protein-pigment complex using a high-resolution crystal structure. Based on this atomistic model, we evaluated the redox potential of P<sub>A</sub>/P<sub>B</sub> by

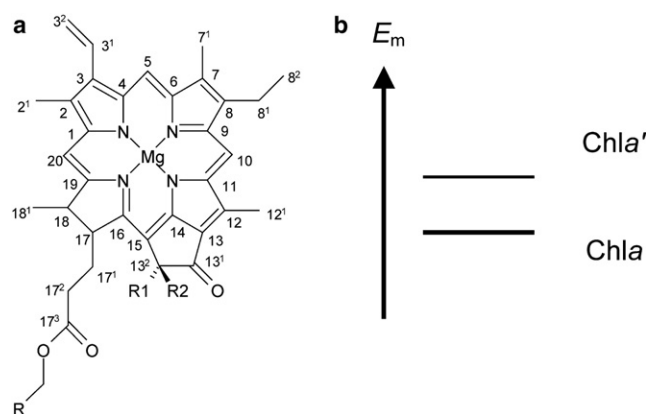


FIGURE 1 (a) Geometry of Chla (R1 = CH<sub>3</sub>COO<sup>-</sup>, R2 = H) and the C13<sup>2</sup> epimer, Chla' (R1 = H, R2 = CH<sub>3</sub>COO<sup>-</sup>). (b)  $E_m$  values of Chla and Chla' in the reference system (e.g., aprotic solvents).

solving the linear Poisson-Boltzmann equation with explicit consideration of the protonation states for all titratable residues.

Second, to gain deeper insights into the electronic structure of P<sub>A</sub>/P<sub>B</sub> Chla'/Chla heterodimer, we performed large-scale QM/MM calculations for the entire PSI protein-pigment complex.

Third, and finally, after confirming the validity of the computational results through comparison with available experimental data, we discussed the atomistic origin that determines the asymmetric distribution of the cationic state of the P<sub>A</sub>/P<sub>B</sub> pair. Technical details of each modeling procedure are summarized as follows.

## Coordinates

The atomic coordinates were taken from the x-ray structure of the PSI protein-pigment complex from *T. elongatus* at 2.5 Å resolution (Protein Data Bank code: 1JB0) (11). Hydrogen atoms were generated and energetically optimized using the CHARMM force field (12). The positions of all nonhydrogen atoms were fixed, and all titratable groups were kept in their standard protonation states; i.e., acidic groups were ionized and basic groups were protonated. For the QM/MM calculations, we added additional counterions to neutralize the whole system.

## Atomic partial charges

Atomic partial charges of the amino acids were adopted from the all-atom CHARMM22 (13) parameter set. The charges of the protonated acidic O atoms were increased successively by +0.5 units to implicitly account for the presence of a proton. Similarly, instead of removing a proton to generate the deprotonated state, the charges of all of the protons of the basic groups of Arg and Lys were successively diminished to a total of 1 unit of charge. For residues for which the protonation states were not available in the CHARMM22 parameter set, appropriate charges were computed (14). For the atomic charges of Chla (except for P<sub>A</sub>/P<sub>B</sub>) and quinones, we used atomic partial charges from previous studies on PSI (15–17); the charges were determined by fitting the surrounding electrostatic potential of these molecules using the RESP procedure (18). The charges of equivalent H atoms (e.g., three H atoms of methyl group) were averaged. The electronic wave functions were calculated after geometry optimization with the DFT module in JAGUAR (19) (B3LYP/LACVP\*) (see Table S1 in the Supporting Material).

## Computation of redox potential $E_m(\text{Chla})$

Our computation was based on the electrostatic continuum model, where the linear Poisson-Boltzmann equation was solved using the MEAD

program (20). To facilitate direct comparisons with previous computational results, identical computational conditions and parameters such as atomic partial charges and dielectric constants were used (21,22). The redox states of all other cofactors (e.g., A<sub>-1</sub> and A<sub>0</sub> Chla, and A<sub>1</sub> quinone) were kept in their neutral charge states during the redox titration of each Chla. We considered F<sub>X</sub>, F<sub>A</sub>, and F<sub>B</sub> in the oxidized charge state [Fe<sub>4</sub>S<sub>4</sub>(SCH<sub>3</sub>)<sub>4</sub>]<sup>2-</sup> for the wild-type PSI as in previous studies (15–17). The ensemble of the protonation patterns was sampled using the Monte Carlo method with the Karlsberg program ([\(http://agknapp.chemie.fu-berlin.de/karlsberg/\(1999\)\)](http://agknapp.chemie.fu-berlin.de/karlsberg/(1999))) (23). The dielectric constants were set to  $\epsilon_p = 4$  inside the protein and  $\epsilon_w = 80$  for water.

All computations were performed at 300 K, pH 7.0, and an ionic strength of 100 mM. The linear Poisson-Boltzmann equation was solved using a three-step grid-focusing procedure at resolutions of 2.5, 1.0, and 0.3 Å. The Monte Carlo sampling for a redox-active group yielded the probabilities [A<sub>ox</sub>] and [A<sub>red</sub>] of the two redox states of molecule A. The shifts in  $E_m(\text{Chla}')$  and  $E_m(\text{Chla})$  due to the PSI protein environment were evaluated using the Nernst equation. A bias potential was applied to obtain an equal amount of both redox states ([A<sub>ox</sub>] = [A<sub>red</sub>]), yielding the redox midpoint potential  $E_m$  as the resulting bias potential. For convenience, the computed  $E_m$  was represented in millivolt accuracy and the last digit was not considered to be significant.

## QM/MM calculations

In all QM/MM calculations reported here, we employed the so-called electrostatic embedding QM/MM scheme. In all the QM/MM calculations, we used the QSITE (24) program code. The electrostatic and steric effects created because of the complex PSI architecture were explicitly considered in all calculations. Owing to the large system size of PSI, the QM region was limited to the P<sub>A</sub>/P<sub>B</sub> Chla'/Chla heterodimer for simplicity, whereas the other protein units and all cofactors were approximated by the MM force field. Because the atomic partial charges were optimized (e.g., A<sub>-1</sub> and A<sub>0</sub> Chla, and A<sub>1</sub> quinone), the QM/MM partition was accurate enough to describe the electronic structure of the [P<sub>A</sub>/P<sub>B</sub>]<sup>•+</sup> Chla'/Chla heterodimer. To reliably determine the cationic character of the [P<sub>A</sub>/P<sub>B</sub>]<sup>•+</sup> heterodimer, we employed the unrestricted DFT method with the B3LYP functional and LACVP\* basis sets. The [P<sub>A</sub>/P<sub>B</sub>]<sup>•+</sup> heterodimer geometry was refined by the constrained QM/MM optimizations; for the surrounding MM protein environment, the atomistic coordinates were exactly fixed with the original x-ray coordinates. After obtaining the stable geometry of the QM fragment, we determined the ESP charges for the cationic state of the [P<sub>A</sub>/P<sub>B</sub>]<sup>•+</sup> heterodimer in the presence of the entire group of PSI atomic coordinates (see Table S1).

## RESULTS AND DISCUSSION

### P<sub>A</sub><sup>•+</sup>/P<sub>B</sub><sup>•+</sup> ratio and spin-density distribution in wild-type PSI

The P<sub>A</sub><sup>•+</sup>/P<sub>B</sub><sup>•+</sup> ratio was calculated to be 27.9:72.1 (Table 1), demonstrating that the cationic state is stabilized more in P<sub>B</sub> than in P<sub>A</sub>: this should result in the value of  $E_m(\text{P}_B)$  being lower than that of  $E_m(\text{P}_A)$ . The P<sub>A</sub><sup>•+</sup>/P<sub>B</sub><sup>•+</sup> ratio of 27.9:72.1 was considerably close to the charge-distribution ratio of 33:67 obtained from FTIR studies of PSI from *Synechocystis* sp. PCC 6803 (6). The calculated spin-density distribution over P<sub>A</sub>/P<sub>B</sub> was 22.4:77.6 (Table 1), which shows greater asymmetry than the ratio of the charge distribution (i.e., P<sub>A</sub><sup>•+</sup>/P<sub>B</sub><sup>•+</sup>), a fact already pointed out previously in PSII (25,26). The obtained value was in good agreement with the experimental values of 25:75 (4) and

**TABLE 1** Values of  $E_m(P_A)$ ,  $E_m(P_B)$  (in mV),  $P_A^{\bullet+}/P_B^{\bullet+}$  ratios, and spin-density distributions in the PSI protein (in %)

(Factor)		$E_m$ shift (versus reference)		Charge		Spin	
		$P_A$	$P_B$	$P_A^{\bullet+}$	$P_B^{\bullet+}$	$P_A$	$P_B$
	Wild-type	29*	27	27.9	72.1	22.4	77.6
(1)	T743V [H-bond]	20*	28	32.2	67.8	26.9	73.1
(2)	CH <sub>3</sub> COO– deleted [Epimer]			32.2	67.8	29.7	70.3
(3)	$\Delta$ (Arg-A750/Ser-B734) [PsaA/PsaB pair]			30.6	69.4	25.0	75.0
(4)	$\Delta$ (A <sub>-1A</sub> /A <sub>-1B</sub> ) [Cofactor]			24.0	76.0	18.7	81.3

The symbol  $\Delta$  stands for deletion of atomic charges of the residues/groups.

\*Because  $E_m(\text{Chl}a')$  in the reference model system is unknown, only the  $E_m$  shift was calculated. An actual  $E_m(\text{Chl}a')$  may be higher than  $E_m(\text{Chl}a)$  because  $\text{Chl}a'$  is thermodynamically less stable than  $\text{Chl}a$  (9).

25:75–20:80 of PSI from spinach (7) and 15:85 of PSI from *T. elongatus* (8) (note: according to another interpretation of the *T. elongatus* data (8), the ratio of 25:75–30:70 may be possible (9)).

The PSI protein environment shifted the  $E_m$  values of  $P_A/P_B$  only marginally from those of the reference model system (Table 1). The shifts were essentially the same for  $P_A$  and  $P_B$ . However, the resulting  $E_m$  values for the  $P_A/P_B$  molecules must be different because of the difference between  $E_m(\text{Chl}a')$  and  $E_m(\text{Chl}a)$  in the reference model system. Although the difference between  $E_m(\text{Chl}a')$  and  $E_m(\text{Chl}a)$  is not known so far, we infer that the former may be higher than the latter because  $\text{Chl}a'$  is thermodynamically less stable than  $\text{Chl}a$  (Fig. 1 b) (9).

### Influence of H-bond on the $P_A^{\bullet+}/P_B^{\bullet+}$ ratio

The –OH group of Thr-A743 can form an H-bond with the 13<sup>1</sup>-keto group of  $P_A$ , whereas the corresponding H-bond is absent in  $P_B$ . A mutation of Thr-A743 to Val would result in the loss of the H-bond (27,28). Using the wild-type PSI crystal structure, we modeled the T(A743)V PSI by substituting the –OH side chain group of Thr with –CH<sub>3</sub> (followed by geometry optimization of the A743 side chain whereas all of the other parts remained fixed).

$E_m(P_A)$  was lowered by ~10 mV upon the T(A743)V mutation whereas  $E_m(P_B)$  remained unchanged (Table 1). The marginal downshift in  $E_m(P_A)$  was in agreement with a relatively weak H-bond of Thr-A743, as pointed out in spectroscopic studies (29). As  $E_m(P_A)$  was lowered (i.e.,  $P_A^{\bullet+}$  was stabilized), the calculated  $P_A^{\bullet+}/P_B^{\bullet+}$  ratio was significantly shifted and the population of  $P_A^{\bullet+}$  increased from 27.9 in the wild-type PSI to 32.2 in the T(A743)V PSI (Table 1). This observed  $P_A^{\bullet+}$  population shift is in agreement with 1), the previous proposal that deletion of the H-bond leads to a downshift in  $E_m(P_A)$  (27), and 2), the experimentally observed relocation of ~14–18% of the cationic state from  $P_B$  to  $P_A$  upon T(A743)V mutation in PSI from *Chlamydomonas reinhardtii* (28). The slightly smaller relocation of the cationic state (i.e., an increase in  $P_A^{\bullet+}$  by 5%) in our study is possibly due to 1), the difference between the used T(A743)V PSI model structure where

the –OH group of Thr was replaced with –CH<sub>3</sub>, without altering the other parts of the atomic coordinates (to avoid an uncertainty of prediction of the protein structure), or 2), the difference of the PSI proteins between *T. elongatus* PSI (corresponds to the crystal structure (2)) and the *Chlamydomonas reinhardtii* PSI. As  $E_m(P700)$  differs by up to ~70 mV among different species (30), the  $P_A/P_B$  moiety may be slightly different among different species.

The individual values of  $E_m(P_A)$  and  $E_m(P_B)$  are not known experimentally due to the presence of their coupling. It is particularly difficult to determine  $E_m(P_A)$  because of the small amount of  $P_A^{\bullet+}$  compared with  $P_B^{\bullet+}$ . Our study demonstrates that shifts in  $E_m(P_A)$  alter the distribution of the cationic (spin) state over  $P_A/P_B$  as reported in mutational studies (27,28).

### Influence of C13<sup>2</sup> epimer $\text{Chl}a'$ on $P_A^{\bullet+}/P_B^{\bullet+}$ ratio

The asymmetric charge distribution over  $P_A/P_B$  may also result from the asymmetry of the molecular geometry in  $P_A/P_B$ . The methyl-ester (CH<sub>3</sub>COO–) groups in  $\text{Chl}a'$  and  $\text{Chl}a$  are oppositely orientated with respect to the chlorin plane. Except for this methyl-ester orientation difference, the molecular structures of  $P_A$  and  $P_B$  are essentially identical (2).

To investigate this orientation difference on the  $P_A^{\bullet+}/P_B^{\bullet+}$  ratio, it would have been more relevant to replace  $\text{Chl}a'$  of  $P_A$  with  $\text{Chl}a$ . Unfortunately, a replacement of  $\text{Chl}a'$  of  $P_A$  with  $\text{Chl}a$  leads to unreasonable contacts with Tyr-A603, Gly-A739, Thr-A742, and Thr-A743. As an alternative, we substituted the CH<sub>3</sub>COO– groups with H in both  $P_A$  and  $P_B$  (deletion of CH<sub>3</sub>COO–), and calculated the  $P_A^{\bullet+}/P_B^{\bullet+}$  ratio. Upon deletion of the CH<sub>3</sub>COO– groups the  $P_A^{\bullet+}$  population increases by ~5% relative to the wild-type PSI, resulting in a  $P_A^{\bullet+}/P_B^{\bullet+}$  ratio of 32.2:67.8 (Table 1). Thus, the orientation difference in  $\text{Chl}a'/\text{Chl}a$  significantly influences the  $P_A^{\bullet+}/P_B^{\bullet+}$  ratio in the PSI protein environment.

Under vacuum conditions, the  $P_A/P_B$  heterodimer yielded a  $P_A^{\bullet+}/P_B^{\bullet+}$  ratio of 41.5:58.5 (Table 2), which indicates a considerably delocalized cationic state distribution over  $P_A/P_B$  in the absence of the PSI protein environment. The

**TABLE 2** Values of  $P_A^{\bullet+}/P_B^{\bullet+}$  ratios and spin-density distributions in vacuum (in %)

	Charge		Spin	
	$P_A^{\bullet+}$	$P_B^{\bullet+}$	$P_A$	$P_B$
Wild-type	41.5	58.5	38.1	61.9
CH <sub>3</sub> COO– deleted	45.5	54.5	46.2	53.8

deletion of CH<sub>3</sub>COO– from P<sub>A</sub>/P<sub>B</sub> delocalized the cationic state, giving a  $P_A^{\bullet+}/P_B^{\bullet+}$  ratio of 45.5:54.5 (Table 2); i.e., the cationic state is almost equally distributed over P<sub>A</sub>/P<sub>B</sub>. It can be concluded that in the absence of the PSI protein environment, the orientation of the CH<sub>3</sub>COO– group in P<sub>A</sub> is predominantly responsible for the  $P_A^{\bullet+}/P_B^{\bullet+}$  ratio (Table 3).

### Influence of PsaA/PsaB symmetrical residue pairs on the $P_A^{\bullet+}/P_B^{\bullet+}$ ratio

The protein environment, in particular the charged residues, contribute to  $E_m$  shifts of the redox active site significantly. Because the  $E_m$  difference  $E_m(P_A) - E_m(P_B)$  ( $= \Delta E_m$ ) is a key factor that can alter the  $P_A^{\bullet+}/P_B^{\bullet+}$  ratio (27) (Fig. 2), it is important to clarify the contributions of residues, in particular those located in the PsaA/PsaB heterodimer subunits.

Arg-A750, located on the luminal side (Fig. 3 a), upshifted  $E_m(P_A)$  the most by 65 mV, due to its positively charged protonated state (Table 4). The Arg-A651 on the lumen side and Arg-A728 near F<sub>X</sub>, both upshifted  $E_m(P_A)$  by 35 mV. Arg-A728 is ~20 Å away from P<sub>A</sub>/P<sub>B</sub>, but its electrostatic influence on  $E_m(P_A)$  and  $E_m(P_B)$  is significant because of the complete absence of other titratable residues in the region between P<sub>A</sub>/P<sub>B</sub> and F<sub>X</sub> (Fig. 3 d).

As both Arg-A651 and Arg-A728 concomitantly increase  $E_m(P_A)$  and  $E_m(P_B)$  with almost the same magnitude (Table 4), these residues were not responsible for the asymmetric distribution of  $P_A^{\bullet+}/P_B^{\bullet+}$ . Furthermore, according to the protein sequence alignment (with the CLUSTAL program (31)), Arg-A651 and Arg-A728 in PsaA are conserved as

**TABLE 3** Analysis of factors (listed in Table 1) that differentiate the populations of  $P_A^{\bullet+}$  and  $P_B^{\bullet+}$  in the PSI protein environment (in %)

	Charge		Spin	
	$P_A^{\bullet+}$	$P_B^{\bullet+}$	$P_A$	$P_B$
Wild-type	27.9	72.1	22.4	77.6
(1) + (2)	37.0	63.0	35.1	64.9
(1) + (3)	35.6	64.4	30.5	69.5
(1) + (2) + (3)	40.5	59.5	39.1	60.9

Factors (1) T743V (deletion of a H-bond with P<sub>A</sub>), (2) CH<sub>3</sub>COO– substitution with –H (deletion of the Chl<sub>a</sub>/Chl<sub>a</sub> difference), and (3) deletion of charges of PsaA/PsaB residue pairs responsible for the  $E_m(P_A)/E_m(P_B)$  difference.

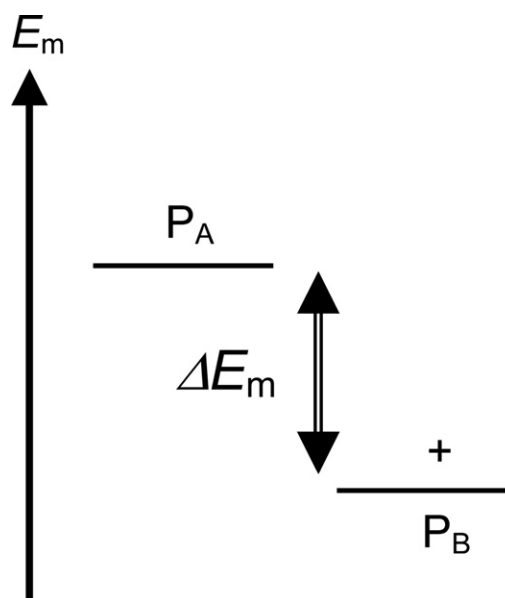


FIGURE 2 Relationship between  $E_m$  and population of the cationic state over the P<sub>A</sub>/P<sub>B</sub> pair. The + sign indicates a population of the energetically distributed cationic state owing to the  $E_m$  levels.  $\Delta E_m = E_m(P_A) - E_m(P_B)$ .

Arg-B627 and Arg-B712 in PsaB, respectively, which also upshifts  $E_m(P_A)$  and  $E_m(P_B)$  (Table 4).

The same argument also holds true for the  $E_m$  downshifting residues, which are mainly acidic residues (Table 5). Asp-B444 significantly downshifted  $E_m(P_A)$  by 90 mV and  $E_m(P_B)$  by 63 mV; and its counterpart in PsaA, Asp-A463, downshifted  $E_m(P_A)$  by 67 mV and  $E_m(P_B)$  by 98 mV. Thus, the influence of Asp-B444 on  $\Delta E_m$  is completely compensated for by the influence of the counterpart Asp-A463.

To clarify how the PSI protein environment differentiates  $P_A^{\bullet+}/P_B^{\bullet+}$ , it is not sufficient to search for the residue that induces large changes in  $E_m$  values, instead it is important to find a residue pair of PsaA/PsaB that increases  $\Delta E_m$  (Fig. 2). Bearing this in mind, we found only a few residue pairs that contribute to nonzero values of  $\Delta E_m$ . The residue pair, Arg-A750/Ser-B734, increased  $\Delta E_m$  by 17 mV (Table 6). Note that the residue pair is fully conserved in cyanobacteria and green plants (Fig. 4). The Arg-A750/Ser-B734 pair is located near P<sub>A</sub>/P<sub>B</sub> on the lumen side (Fig. 3 c). Indeed, Arg-A750 was already mentioned as the residue that upshifted  $E_m(P_A)$  the most among all residues in PSI (Tables 4 and 5) whereas its counterpart is an uncharged residue, Ser.

In the absence of the atomic charges of Arg-A750/Ser-B734, we obtained the  $P_A^{\bullet+}/P_B^{\bullet+}$  ratio of 30.6:69.4; in which the  $P_A^{\bullet+}$  population has increased by ~3%, with respect to wild-type PSI (Table 1). This result indicates that, in turn, the Arg-A750/Ser-B734 pair contributes to increase the  $P_B^{\bullet+}$  population in the wild-type PSI by increasing  $\Delta E_m$ .

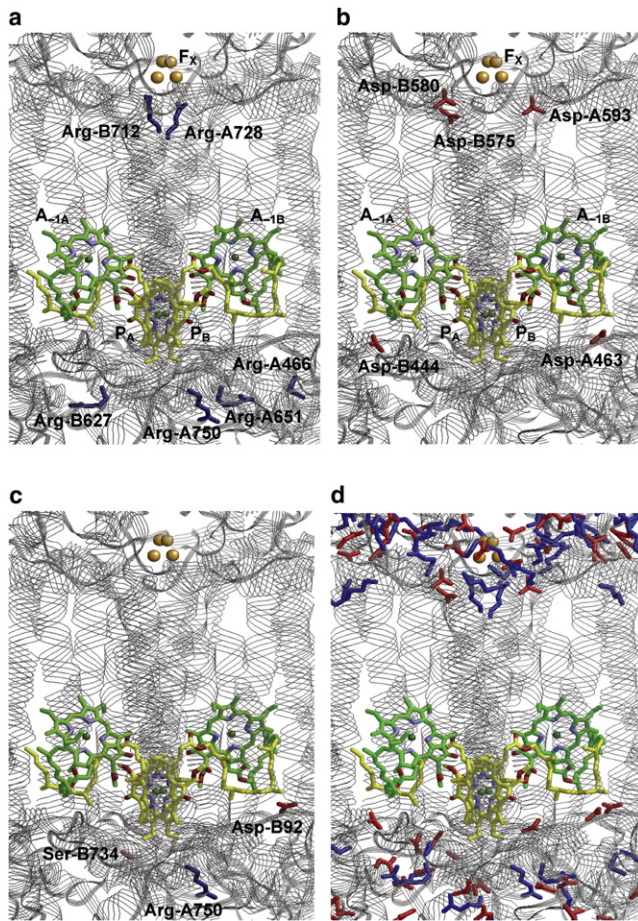


FIGURE 3 Arrangement of residues in PsaA/PsaB of PSI. (Blue and red sticks) Side chains of basic and acidic residues, respectively. (a) Residues increasing  $E_m(P_A)$  or  $E_m(P_B)$ . (b) Residues decreasing  $E_m(P_A)$  or  $E_m(P_B)$ . (c) Residue pairs enhancing  $E_m(P_A) > E_m(P_B)$ . (d) All acidic and basic residues in PsaA/PsaB.

The Arg-A750/Ser-B734 residue pair contributes the most to  $\Delta E_m$  among all PsaA/PsaB residue pairs; however, it increases  $\Delta E_m$  only by 17 mV (Table 6). The second most contributing residue pair —/Asp-B92, in which the corresponding residue in PsaA is absent among cyanobacteria and green plants (Fig. 4), contributes 9 mV to  $\Delta E_m$  (Table 6). Hence, in comparison with the much larger influence of a number of D1/D2 residue pairs on the  $E_m(P_{D1})/E_m(P_{D2})$

TABLE 4 Residues that shift  $E_m(P_A)$  and  $E_m(P_B)$  in the PSI protein environment (mV)

Residue	$E_m(P_A)$ shift			$E_m(P_B)$ shift		
	Side chain	Backbone	Total	Side chain	Backbone	Total
Increasing $E_m(P_A)$ and $E_m(P_B)$						
Arg-A750	53	12	65	Arg-A651	60	55
Arg-A651	42	-7	35	Arg-A750	30	36
Arg-A728	39	-4	35	Arg-A466	32	35
Arg-B627	36	-3	33	Arg-B712	36	32
Arg-B712	34	-3	31	Arg-A728	35	32

TABLE 5 Residues that shift  $E_m(P_A)$  and  $E_m(P_B)$  in the PSI protein environment (mV)

Residue	$E_m(P_A)$ shift			$E_m(P_B)$ shift			
	Side chain	Backbone	Total	Side chain	Backbone	Total	
Decreasing $E_m(P_A)$ and $E_m(P_B)$							
Asp-B444	-94	4	-90	Asp-A463	-102	4	-98
Asp-A463	-70	3	-67	His-B660	-70	6	-64
His-A680	-72	5	-67	Asp-B444	-66	3	-63
A <sub>-1A</sub>			-65	F <sub>X</sub>			-47
F <sub>X</sub>			-48	Asp-B575	-42	0	-42
Asp-B575	-41	0	-42	A <sub>-1B</sub>			-41
Asp-A593	-33	-2	-35	Asp-B580	-31	-2	-33
His-B660	-31	0	-31	His-A680	-31	-1	-32
Asp-B580	-28	-2	-30	Asp-A593	-29	-2	-31

difference in PSII (10), the protein environments of PsaA and PsaB in PSI are quite similar in their electrostatic characters.

The residue pairs Arg-A750/Ser-B734 and —/Asp-B92 are responsible for  $\Delta E_m$  in wild-type PSI. Mutations of these residues would produce other protonation patterns of the titratable residues of PSI to compensate for the induced changes (e.g., charges or protein conformations). Unless the protonation pattern of the titratable residues and the protein conformation remain unchanged upon the corresponding mutations, mutational studies do not directly correspond to our results of the wild-type PSI.

### Differences in the two accessory Chl<sub>a</sub> pairs A<sub>-1A</sub> and A<sub>-1B</sub>

There are also pairs that contribute to decrease  $\Delta E_m$  and facilitate an accumulation of  $P_B^{\bullet+}$ . Unexpectedly, the most influential was the accessory Chl<sub>a</sub> pair, A<sub>-1A</sub> and A<sub>-1B</sub>, which decreased  $\Delta E_m$  by 28 mV (Table 7). It was surprising, because both A<sub>-1A</sub> and A<sub>-1B</sub> are identical molecules, Chl<sub>a</sub>, and the methyl-ester groups of P<sub>A</sub>/P<sub>B</sub>, i.e., the region causing the Chl<sub>a</sub>/Chl<sub>b</sub> difference, is sufficiently far from the interface between P<sub>A</sub>/P<sub>B</sub> and A<sub>-1A</sub>/A<sub>-1B</sub>.

As expected from the  $\Delta E_m$  value, eliminating the atomic charges of A<sub>-1A</sub> and A<sub>-1B</sub> resulted in the decrease in the

TABLE 6 PsaA/PsaB residue pairs responsible for  $\Delta E_m (= E_m(P_A) - E_m(P_B))$ , see Fig. 2 (mV)

Residue	PsaA		PsaB		$\Delta E_m$
	$E_m(P_A)$	$E_m(P_B)$	Residue	$E_m(P_A)$ / $E_m(P_B)$	
$\Delta E_m$ increasing pairs (i.e., pairs that contribute to accumulation of $P_B^{\bullet+}$ )					
Arg-A750	65	36	Ser-B734	9 / 21	17
—	—	—	Asp-B92	-15 / -24	9

Contribution to  $\Delta E_m$  was obtained as [influence of PsaA on  $E_m(P_A)$ ] + [influence of PsaB on  $E_m(P_A)$ ] - [influence of PsaA on  $E_m(P_B)$ ] - [influence of PsaB on  $E_m(P_B)$ ]. PsaA/PsaB residue pairs in each line were generated from the protein sequence alignment performed with the CLUSTAL program (31) (Fig. 4).

	98	108	118	127	137
PsaA <i>T.elongatus</i>	SNYEAWLADP	TGIKPSAQVV	WPIVGGQIL	NGDVGGGFHG	-IQIT-SGLF
PsaA <i>S.6803</i>	SNYEGWLADP	THIKPSAQVV	WPIVGGQIL	NGDVGGGFHG	-IQIT-SGLF
PsaA <i>C.reinhardtii</i>	SNYEAWLSDP	THIKPSAQVV	WPIVGGQIL	NGDVGGGFQG	-IQIT-SGFF
PsaA <i>spinach</i>	SNYEAWLSDP	THIGPSAQVV	WPIVGGQIL	NGDVGGGFHG	-IQIT-SGFF
	71	81	91	101	111
PsaB <i>T.elongatus</i>	GNFEQWVQDP	VNTRPIAHAI	WDPQFGKAAV	DAFTQAGASN	PVDIAYSGVY
PsaB <i>S.6803</i>	GNFEQWIKDP	LNIRPIAHAI	WDPHFGGAV	NAFTQAGASN	PVNIAYSGVY
PsaB <i>C.reinhardtii</i>	GNFEQWVQDP	VHIRPIAHAI	WDPHFGQPAV	EAFTRGGASG	PVNISTSGVY
PsaB <i>spinach</i>	GNFESWVQDP	LHVRPIAHAI	WDPHFGQPAV	EAFTRGGALG	PVNIAYSGVY
	711	718	727	737	747
PsaA <i>T.elongatus</i>	LKVAPAI---	-QPRALSIIQ	GRAVGVAYHL	LGGIATTWAF	FLARIISVG-
PsaA <i>S.6803</i>	LNVPAPAI---	-QPRALSIIQ	GRAVGVAYHL	LGGIVTTWAF	FLARLSISIG-
PsaA <i>C.reinhardtii</i>	LKVAPAI---	-QPRALSITQ	GRAVGVAYHL	LGGIATTWSF	FLARIISVG-
PsaA <i>spinach</i>	LKVAPAT---	-QPRALSIVQ	GRAVGVTHYL	LGGIATTWAF	FLARIIAVG-
	691	701	711	721	731
PsaB <i>T.elongatus</i>	TPLANLVRWK	DKPVALSIVQ	ARLVGLAHFS	VGYLTYAAF	LIASTAAKFG
PsaB <i>S.6803</i>	TPLANLVRWK	DKPVALSIVQ	ARLVGLAHFT	VGVLTYAAF	LIASTAGKFG
PsaB <i>C.reinhardtii</i>	TPLANLVYWK	DKPVALSIVQ	ARLVGLAHFS	VGYIFTYAAF	LIASTSGRFG
PsaB <i>spinach</i>	TPLANLIRWR	DKPVALSIVQ	ARLVGLAHFS	VGYIFTYAAF	LIASTSGKFG

FIGURE 4 Amino-acid sequences of the PsaA and PsaB subunits of PSI from *T. elongatus*, *Synechocystis* PCC 6803 (*S.6803*), *Chlamydomonas reinhardtii* (*C. reinhardtii*), and spinach. PsaA/PsaB residue pairs in each line were generated from the protein sequence alignment performed with the CLUSTAL program (31).

$P_A^{\bullet+}$  population, shifting the  $P_A^{\bullet+}/P_B^{\bullet+}$  ratio to 24.0:76.0 (Table 1). Thus, the influence of the accessory Chl*a* pair on the  $P_A^{\bullet+}/P_B^{\bullet+}$  ratio as well as  $\Delta E_m$  appears to be significant.

For the first time to our knowledge, in this work it has been found that the difference in the energy contribution of  $A_{-1A}/A_{-1B}$  to  $P_A/P_B$  results from the orientation of the methyl-ester groups of  $A_{-1A}/A_{-1B}$ , which are orientated at an angle of  $\sim 180^\circ$  to each other across the  $C13^2-C13^3$  axis (Fig. 5). Because the methyl-ester groups are situated on the same side of the chlorin plane, the  $A_{-1A}/A_{-1B}$  pair consist of methyl-ester rotamers and not methyl-ester epimers. The carbonyl O atom of  $A_{-1A}$  is 5.4 Å away from the Mg atom of  $P_A$  whereas the corresponding distance is 7.1 Å between  $A_{-1B}$  and  $P_B$  (Fig. 5). Because the carbonyl O

atom is polarized more than the ester O atom, the methyl-ester group of  $A_{-1A}$  can stabilize the cationic  $P_A^{\bullet+}$  state more effectively than that of the  $A_{-1B}$  for the  $P_B^{\bullet+}$  state, thus decreasing  $E_m(P_A)$  relative to  $E_m(P_B)$ . The possible role of the methyl-ester orientation of a Chl*a* in altering the  $E_m$  of another Chl*a* in the neighborhood was originally reported in PSII (32), and our results indicate that the same phenomenon holds true for  $P_A/P_B$  in PSI. Note that a clear discrimination between the  $-O-CH_3$  and O edges of the ester-group in the electron density map was possible at a resolution of  $\sim 2.5$  Å (W. Saenger, Free University of Berlin, personal communication, 2011).

The H-bonding partner for any group that specifies the orientation of the methyl-ester groups of  $A_{-1A}/A_{-1B}$  or cause steric hindrance is absent. By rotating each methyl-ester group in  $A_{-1A}/A_{-1B}$  that is itself rotated by  $180^\circ$  along the  $C13^2-C13^3$  axis, the  $P_A^{\bullet+}/P_B^{\bullet+}$  ratio changed from 27.9:72.1 (wild-type) to 22.4:77.6 (rotated methyl-ester:  $A_{-1A}/A_{-1B}$ , Table 8) and the corresponding spin-density distributions in  $P_A/P_B$  were shifted from 22.4:77.6 to 15.1:84.9, respectively. The spin-density distribution of 15.1:84.9 was considerably shifted from the wild-type PSI value. A similar value of the spin-density distribution (15:85) was reported from EPR studies of PSI from *T. elongatus* (8). As the energy required for rotation of the methyl-ester group is not unusually large (due to the  $sp^3$  carbons) and the H-bonding partner that specifies the orientation of the methyl-ester groups of  $A_{-1A}/A_{-1B}$  is absent, it is reasonable to assume that the  $P_A^{\bullet+}/P_B^{\bullet+}$  ratio and the

TABLE 7 PsaA/PsaB residue pairs responsible for  $\Delta E_m (= E_m(P_A) - E_m(P_B))$ , see Fig. 2 (in mV)

Residue	PsaA		PsaB		$\Delta E_m$
	$E_m(P_A)$	$E_m(P_B)$	Residue	$E_m(P_A)$	
$\Delta E_m$ decreasing pairs (i.e., pairs that contribute to accumulation of $P_A^{\bullet+}$ )					
$A_{-1A}$	-65	-23	$A_{-1B}$	-19	-41
Gln-A657	-4	-2	Asn-B633	18	26

Contribution to  $\Delta E_m$  was obtained as [influence of PsaA on  $E_m(P_A)$ ] + [influence of PsaB on  $E_m(P_A)$ ] - [influence of PsaA on  $E_m(P_B)$ ] - [influence of PsaB on  $E_m(P_B)$ ]. PsaA/PsaB residue pairs in each line were generated from the protein sequence alignment performed with the CLUSTAL program (31) (Fig. 4).

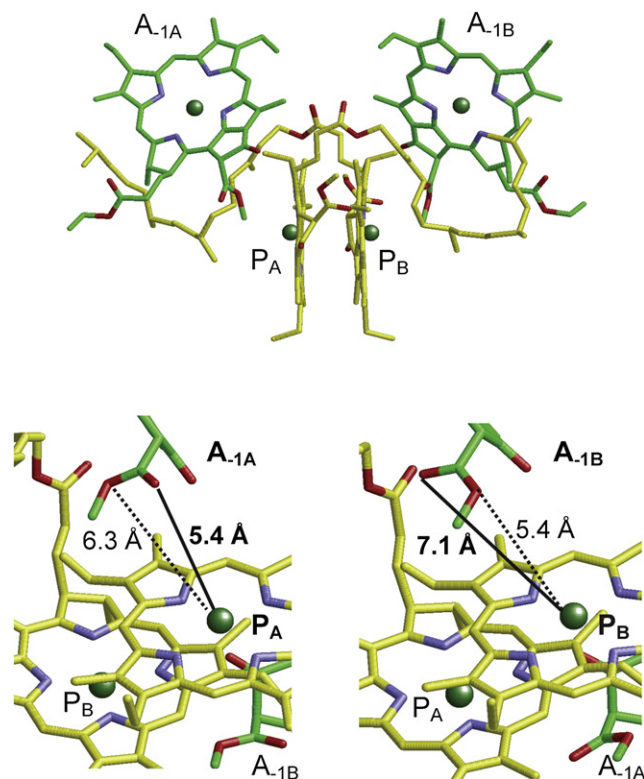


FIGURE 5 Geometry of the accessory Chl  $a$   $A_{-1A}$  and  $A_{-1B}$ . (Solid and dotted lines) Distances between the Mg atom and the O atoms of the carbonyl and ester groups, respectively.

spin-density distribution over  $P_A/P_B$  fluctuates within the ranges given in Table 8. Hence, the orientation of the methyl-ester group in  $A_{-1A}/A_{-1B}$  can affect the  $P_A/P_B$   $\Delta E_m$  and the  $P_A^{\bullet+}/P_B^{\bullet+}$  ratio.

## CONCLUSIONS

The  $P_A^{\bullet+}/P_B^{\bullet+}$  ratio of the  $P_A/P_B$  dimer calculated over the entire PSI protein was 28:72, which was close to the charge-distribution ratio of 33:67 obtained in the FTIR studies of PSI from *Synechocystis* sp. PCC 6803 (6). The calculated spin density, which was asymmetrically distributed over the  $P_A/P_B$  dimer with a ratio of 22:78, was in good agreement with the experimental values of 25:75 (4) and 20:80

**TABLE 8** Influence of the orientation of the methyl-ester group of  $A_{-1A}/A_{-1B}$  on the  $P_A^{\bullet+}/P_B^{\bullet+}$  ratio and spin-density distribution calculated in the PSI protein (in %)

	Charge		Spin	
	$P_A^{\bullet+}$	$P_B^{\bullet+}$	$P_A$	$P_B$
Wild-type	27.9	72.1	22.4	77.6
	[Rotated methyl-ester]			
$A_{-1A}$	26.6	73.4	19.7	80.3
$A_{-1B}$	23.5	76.5	17.4	82.6
$A_{-1A}/A_{-1B}$	22.4	77.6	15.1	84.9

in EPR studies from spinach (7). The Chl  $a'$ /Chl  $a$  difference for  $P_A/P_B$  was revealed to be partially responsible for the larger population of the  $P_B^{\bullet+}$  state, from the methyl-ester deletion simulations. Removal of the H-bond between  $P_A$  and Thr-A743 in T(A743)V mutation resulted in a slight decrease in  $E_m(P_A)$  and a partial movement of the cationic state from  $P_A$  to  $P_B$ , as suggested by mutational studies (27,28).

Conserved PsaA/PsaB pairs, Arg-A651/Arg-B627 and Arg-A728/Arg-B712 upshifted both  $E_m(P_A)$  and  $E_m(P_B)$  by  $\sim 30$  mV, and Asp-A463/Asp-B444 and Asp-A593/Asp-B580 residue pairs downshifted both  $E_m(P_A)$  and  $E_m(P_B)$  in the range  $\sim 30$ –60 mV. The residue pair that led to a notable value of  $\Delta E_m$  (i.e.,  $E_m(P_A) > E_m(P_B)$ ) was Arg-A750/Ser-B734, with a  $\Delta E_m$  of 17 mV, thus contributing to an increase in the  $P_B^{\bullet+}$  population (Note that a simple mutation of the residues would cause a change in the protonation states of the titratable residues in PSI, compensating for changes in the net charges of the mutated sites.). On the other hand, the most influential pair enhancing  $E_m(P_A) < E_m(P_B)$  was the accessory  $A_{-1A}/A_{-1B}$  Chl  $a$  pair, with a  $\Delta E_m$  of 28 mV; this pair contributed to an increase in the  $P_A^{\bullet+}$  population in the original PSI crystal structure. The different influence of  $A_{-1A}$  and  $A_{-1B}$  on  $E_m(P_A)$  and  $E_m(P_B)$  was due to the differences in their methyl-ester orientations. Rotation of the methyl-ester groups alters the  $P_A/P_B$  spin-density distributions from 22:78 to 15:85. The latter value was in agreement with the value of 15:85 measured by EPR for PSI from *T. elongatus* (8).

## SUPPORTING MATERIAL

One table is available at [http://www.biophysj.org/biophysj/supplemental/S0006-3495\(11\)01064-2](http://www.biophysj.org/biophysj/supplemental/S0006-3495(11)01064-2).

We are grateful to Dr. Wolfram Saenger and Dr. Ernst-Walter Knapp for useful discussions.

This research was supported by the Japan Science and Technology Agency PRESTO program (to H.I.); Grant-in-Aid (21770163 to H.I. and 22740276 to K.S.) for Science Research from the Ministry of Education, Science, Sport and Culture of Japan; Special Coordination Fund (to H.I.) for Promoting Science and Technology of MEXT; Takeda Science Foundation (to H.I.); and Kyoto University Step-up Grant-in-Aid for young scientists (to H.I.).

## REFERENCES

- Watanabe, T., M. Kobayashi, ..., N. Murata. 1985. Evidence that a chlorophyll  $a'$  dimer constitutes the photochemical reaction center 1 (P700) in photosynthetic apparatus. *FEBS Lett.* 191:252–256.
- Jordan, P., P. Fromme, ..., N. Krauss. 2001. Three-dimensional structure of cyanobacterial photosystem I at 2.5 Å resolution. *Nature.* 411:909–917.
- Guergova-Kuras, M., B. Boudreaux, ..., K. Redding. 2001. Evidence for two active branches for electron transfer in photosystem I. *Proc. Natl. Acad. Sci. USA.* 98:4437–4442.
- Rigby, S. E. J., J. H. A. Nugent, and P. J. O'Malley. 1994. ENDOR and special triple resonance studies of chlorophyll cation radicals in photosystem 2. *Biochemistry.* 33:10043–10050.

5. Diner, B. A., E. Schlodder, ..., D. A. Chisholm. 2001. Site-directed mutations at D1-His<sup>198</sup> and D2-His<sup>197</sup> of photosystem II in *Synechocystis* PCC 6803: sites of primary charge separation and cation and triplet stabilization. *Biochemistry*. 40:9265–9281.
6. Breton, J., E. Navedryk, and W. Leibl. 1999. FTIR study of the primary electron donor of photosystem I (P700) revealing delocalization of the charge in P700<sup>+</sup> and localization of the triplet character in <sup>3</sup>P700. *Biochemistry*. 38:11585–11592.
7. Davis, I. H., P. Heathcote, ..., M. C. W. Evance. 1993. Modulation analysis of the electron spin echo signals of in vivo oxidized primary donor <sup>14</sup>N chlorophyll centers in bacterial, P870 and P960, and plant photosystem I, P700, reaction centers. *Biochim. Biophys. Acta*. 1143:183–189.
8. Kass, H., P. Fromme, ..., W. Lubitz. 2001. Orientation and electronic structure of the primary donor radical cation P700<sup>+</sup> in photosystem I: a single crystals EPR and ENDOR study. *J. Phys. Chem. B*. 105:1225–1239.
9. Webber, A. N., and W. Lubitz. 2001. P700: the primary electron donor of photosystem I. *Biochim. Biophys. Acta*. 1507:61–79.
10. Saito, K., T. Ishida, ..., H. Ishikita. 2011. Distribution of the cationic state over the chlorophyll pair of photosystem II reaction center. *J. Am. Chem. Soc.* 133:14379–14388.
11. Umena, Y., K. Kawakami, ..., N. Kamiya. 2011. Crystal structure of oxygen-evolving photosystem II at a resolution of 1.9 Å. *Nature*. 473:55–60.
12. Brooks, B. R., R. E. Bruccoleri, ..., M. Karplus. 1983. CHARMM: a program for macromolecular energy minimization and dynamics calculations. *J. Comput. Chem.* 4:187–217.
13. MacKerell, Jr., A. D., D. Bashford, ..., M. Karplus. 1998. All-atom empirical potential for molecular modeling and dynamics studies of proteins. *J. Phys. Chem. B*. 102:3586–3616.
14. Rabenstein, B., G. M. Ullmann, and E.-W. Knapp. 1998. Calculation of protonation patterns in proteins with structural relaxation and molecular ensembles—application to the photosynthetic reaction center. *Eur. Biophys. J.* 27:626–637.
15. Ishikita, H., and E.-W. Knapp. 2003. Redox potential of quinones in both electron transfer branches of photosystem I. *J. Biol. Chem.* 278:52002–52011.
16. Ishikita, H., D. Stehlik, ..., E. W. Knapp. 2006. Electrostatic influence of PsaC protein binding to the PsaA/PsaB heterodimer in photosystem I. *Biophys. J.* 90:1081–1089.
17. Karyagina, I., Y. Pushkar, ..., J. H. Golbeck. 2007. Contributions of the protein environment to the midpoint potentials of the A1 phylloquinones and the F<sub>X</sub> iron-sulfur cluster in photosystem I. *Biochemistry*. 46:10804–10816.
18. Bayly, C. I., P. Cieplak, ..., P. A. Kollman. 1993. A well-behaved electrostatic potential based method using charge restraints for deriving atomic charges: the RESP model. *J. Phys. Chem.* 97:10269–10280.
19. Schrödinger. 2008. JAGUAR, v. 7. Schrödinger, LLC, New York, NY.
20. Bashford, D., and M. Karplus. 1990. pK<sub>a</sub>'s of ionizable groups in proteins: atomic detail from a continuum electrostatic model. *Biochemistry*. 29:10219–10225.
21. Ishikita, H., W. Saenger, ..., E. W. Knapp. 2006. How photosynthetic reaction centers control oxidation power in chlorophyll pairs P680, P700, and P870. *Proc. Natl. Acad. Sci. USA*. 103:9855–9860.
22. Ishikita, H., J. Biesiadka, ..., E. W. Knapp. 2006. Cationic state of accessory chlorophyll and electron transfer through pheophytin to plastoquinone in photosystem II. *Angew. Chem. Int. Ed. Engl.* 45:1964–1965.
23. Rabenstein, B., and E. W. Knapp. 2001. Calculated pH-dependent population and protonation of carbon-monoxo-myoglobin conformers. *Biophys. J.* 80:1141–1150.
24. Schrödinger. 2010. QSITE, v. 5.6. Schrödinger, LLC, New York, NY.
25. Plato, M., N. Krauss, ..., W. Lubitz. 2003. Molecular orbital study of the primary electron donor P700 of photosystem I based on a recent x-ray single crystal structure analysis. *Chem. Phys.* 294:483–499.
26. Okubo, T., T. Tomo, ..., T. Noguchi. 2007. Perturbation of the structure of P680 and the charge distribution on its radical cation in isolated reaction center complexes of photosystem II as revealed by Fourier transform infrared spectroscopy. *Biochemistry*. 46:4390–4397.
27. Witt, H., E. Schlodder, ..., W. Lubitz. 2002. Hydrogen bonding to P700: site-directed mutagenesis of threonine A739 of photosystem I in *Chlamydomonas reinhardtii*. *Biochemistry*. 41:8557–8569.
28. Li, Y., M.-G. Lucas, ..., K. Redding. 2004. Mutation of the putative hydrogen-bond donor to P<sub>700</sub> of photosystem I. *Biochemistry*. 43:12634–12647.
29. Hastings, G., V. M. Ramesh, ..., A. Webber. 2001. Primary donor photo-oxidation in photosystem I: a reevaluation of (P700<sup>+</sup>-P700) Fourier transform infrared difference spectra. *Biochemistry*. 40:12943–12949.
30. Nakamura, A., T. Suzawa, ..., T. Watanabe. 2011. Species dependence of the redox potential of the primary electron donor P700 in photosystem I of oxygenic photosynthetic organisms revealed by spectroelectrochemistry. *Plant Cell Physiol.* 52:815–823.
31. Higgins, D. G., J. D. Thompson, and T. J. Gibson. 1996. Using CLUSTAL for multiple sequence alignments. *Methods Enzymol.* 266:383–402.
32. Ishikita, H., B. Loll, ..., E. W. Knapp. 2005. Tuning electron transfer by ester-group of chlorophylls in bacterial photosynthetic reaction center. *FEBS Lett.* 579:712–716.